1987-07

A Fiber-optic Interferometric Seismometer

Gardner, D.L.

Journal of Lightwave Technology, Volume LT-5, No. 7, July 1987
http://hdl.handle.net/10945/44062

A Fiber-Optic Interferometric Seismometer

D. L. GARDNER, T. HOFLER, S. R. BAKER, R. K. YARBER, AND S. L. GARRETT

Abstract—**A fiber-optic interferometric sensor has been developed which consists of a seismic mass of 520 gm supported by two rubber mandrels, each wound with a single layer of single-mode optical fiber 6.5 m long. One end of each fiber is cleaved to enhance reflection. The other ends are interconnected via a fiber-to-fiber 3-dB coupler, forming a Michelson interferometer. When the case of the sensor is displaced, the fiber around one mandrel extends in length while the other contracts. The resulting "push–pull" mechanical operation of the sensor allows both legs of the interferometer to be active, providing good common mode rejection of spurious effects, as a reference leg is not required. This, together with the fact that the light traverses each leg of a Michelson interferometer twice due to reflection, provides the sensor with four times the sensitivity of a conventionally constructed interferometric sensor. Sensitivities of 8500 rad of optical phase shift per micrometer of case displacement have been measured above the mass-spring resonance, where the sensor operates as a seismometer. Below resonance the sensor operates as an accelerometer with a measured sensitivity of 10 500 rad/g, the highest reported to date. Including both thermodynamic and demodulator noise sources ($\approx 10\ \mu rad/\sqrt{Hz}$), below resonance the sensor has a detection threshold of 1 ng/$\sqrt{Hz}$, a 20-dB improvement over the best existing conventional low noise vibration sensors.**

I. Introduction

MUCH of the initial enthusiam surrounding the application of optical fiber technology to sensor systems was generated by the potential for high sensitivity using interferometry coupled with the possibility of an all optical system which would take advantage of fiber-optic telemetry, thereby eliminating the need for parallel electrical systems to power and condition the electronic outputs of the sensors. The promise of high sensitivity was not based on the intrinsic sensitivity of optical fibers to physical stimuli but on the fact that optical phase shifts on the order of microradians could be resolved and optical path lengths of tens or hundreds of meters could be incorporated in sensors of modest physical dimensions. That combination of high interferometric demodulator resolution and long optical path length led to the possibility of measurements with resolutions on the order of a part in 10^{11} to 10^{14}. In addition to measurement of conventional physical parameters [1], [2] such as temperature, pressure, etc., fiber-optic sensors were suggested for such unusual measurements as the detection of cosmologically generated gravitational waves [3].

Manuscript received December 17, 1986; revised March 11, 1987. This work was supported by the Office of Naval Technology, the Office of Naval Research, and the Naval Postgraduate School Foundation Research Program.

The authors are with the Physics Department, Naval Postgraduate School, Monterey, CA 93943.

IEEE Log Number 8714767.

With time it became apparent that such high sensitivities might not lead to practical devices, as microradian optical interferometric demodulators were not easy to produce outside the laboratory. In addition, the optical fiber was found to be as sensitive to most extraneous physical parameters as it is to the parameter which it was designed to detect, making it difficult to stabilize a "reference fiber" in one arm of a conventional interferometer against fluctuations in ambient conditions such as temperature, static pressure, accelerations, etc., which also induced changes in the optical path length. This paper describes a successful attempt to design, fabricate, and test an interferometric entirely fiber-optical seismic sensor, which is: easy to construct, using less than 10 m of optical fiber; is differential, so as to eliminate the necessity for a reference optical path; can be modeled easily, so it lends itself to modification for differing applications; and has a vibro-acoustic optical sensitivity which is extremely high and an intrinsic noise which is of the same order or lower than that of current practical optical interferometric demodulators.

II. Seismic Sensors

Sensors used for the measurement of mechanical motion (e.g., displacement, velocity, or acceleration) fall into two basic catagories. Those which make a measurement with respect to some fixed point in space are known as fixed reference instruments. In many applications a fixed reference is not available and a simple mass–spring system (simple harmonic oscillator) is used which exploits the inertial properties of the mass to act as the reference for some strain measuring transducer whose output can be interpeted via simple physical models to deduce mechanical motion. In conventional seismic sensors the strain is usually detected by some piezoelectric or piezoresistive element, as is common with accelerometers; a capacitor or inductive displacement sensing element, common in sieismometers; or an electrodynamic displacement rate transducer, common in geophones. Such inertial instruments based on simple harmonic oscillators are called seismic transducers [4].

While the function of a strain gage is relatively simple, in that a change in the length of the spring which supports the mass is converted into an electronic signal, the distinction between seismometers (displacement sensors), accelerometers, and geophones (velocity sensors) is frequency dependent. For sinusoidal excitation, the parameters measured by these three devices are related by various integer powers of frequency, for instance

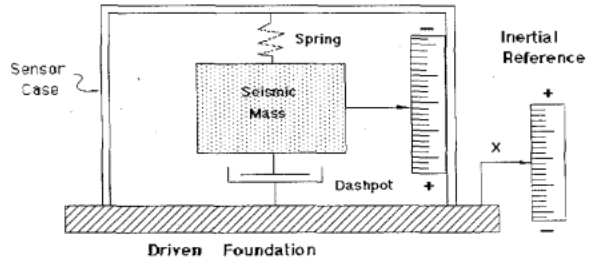

Fig. 1. Diagram of a generic seismic instrument. After Harris and Crede [4].

$$\alpha(t) = -\omega^2 X(t) \tag{1}$$

where

ω radian frequency,
α acceleration,
X displacement.

The devices are similar in that each is fundamentally a simple harmonic oscillator system, and are distinguished by their frequency range of operation. The response of this generic seismic instrument (Fig. 1) is given by Harris [4] as:

$$\frac{\delta_0}{X_0} = \frac{\left(\frac{\omega}{\omega_n}\right)^2}{\sqrt{\left[1 - \left(\frac{\omega}{\omega_n}\right)^2\right]^2 + \left(2\xi\,\frac{\omega}{\omega_n}\right)^2}} \tag{2}$$

where

δ_0 relative displacement between the seismic mass and case,
ξ damping ratio,
ω_n natural frequency.

Variables with the subscript zero are the peak values of the quantity that is assumed to be varying sinusoidally. Assuming small damping ($\xi << 1$), at frequencies well above resonance, or $\omega >> \omega_n$, the mass is nearly stationary with respect to an inertial reference frame. The relative displacement of the case and seismic mass δ_0 is transduced by the sensor and is proportional to the foundation displacement. With this operating frequency constraint, the device is a seismometer and δ_0 is independent of frequency.

Using (1), (2) can be written as

$$\frac{\delta_0}{\alpha_0} = -\frac{1}{\omega_n^2}\left[\frac{1}{\sqrt{\left[1 - \left(\frac{\omega}{\omega_n}\right)^2\right]^2 + \left(2\xi\,\frac{\omega}{\omega_n}\right)^2}}\right]. \tag{3}$$

At frequencies below resonance, $\omega << \omega_n$, δ_0 is proportional to α_0, and δ_0 becomes a measure of the acceleration, with sensitivity which is inversely proportional to the square of the natural frequency or directly proportional to the seismic mass.

The geophone, which measures the velocity of the foundation, can be constructed to operate in either of the two regimes described above by appropriate electronic differentiation or integration of the strain gage output. However, a common means of constructing a conventional geophone is to attach to the foundation a wire coil which moves within a suspended magnetic seismic mass, so that the voltage generated by their relative motion is directly proportional to the velocity. In an interferometric optical seismometer, geophone operation can be produced by processing the optical signal as a fringe rate for operation above resonance [5].

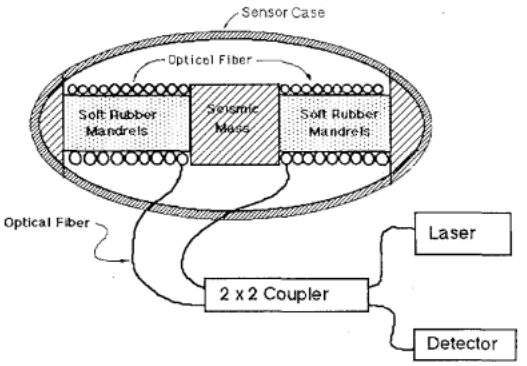

Fig. 2. Diagram of the fiber-optic interferometric seismometer. The soft rubber mandrels are circumferentially wrapped with optical fiber. In the actual sensor, the coupler will be in the case.

III. Interferometric Seismometer

A. Block Diagram

Fig. 2 is a schematic representation of the seismometer we have designed and tested. For reasons which will be addressed in detail shortly, the sensor consists of two fiber-wrapped rubber springs which support a seismic mass. In the actual sensor the coupler is contained within the case. The block diagram of the sensor, test fixture, and associated instrumentation is shown in Fig. 3.

The "springs" supporting the seismic mass are right circular cylinders fabricated from soft silicone rubber [6], each wrapped with optical fiber which acts as one arm of the optical fiber interferometer. The function of the rubber mandrels is to transform relative longitudinal motion between the case and mass into fiber strain. When operated in the seismometer limit $\omega << \omega_n$ the mass (Fig. 1) remains approximately stationary as the foundation moves. This forces one of the mandrels to shorten and the other to lengthen, in a push–pull configuration. The rubber is effectively incompressible. Since the volume of the rubber is conserved, a change in height of the mandrel induces a change in circumference. The optical fiber is initially wrapped around the mandrel under tension and thus will respond to both increases and decreases in mandrel circumference. The push–pull effect is one reason for the seismometer's high sensitivity. Its sensitivity is further enhanced by using the Michelson configuration for the interferometer, as the light passes through each sensor coil twice.

The sensitivity of this sensor to transverse motion is in

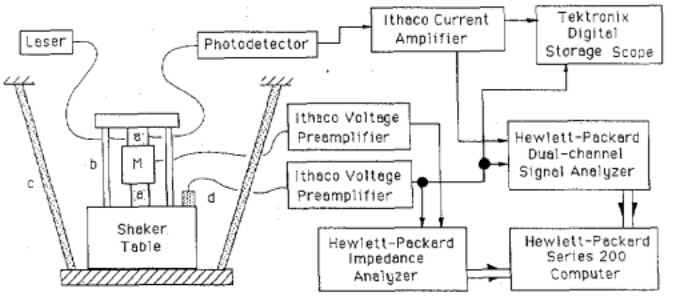

Legend

a - Soft rubber mandrels wrapped with optical fiber
b - Test fixture supporting towers
c - Vibration isolation supports
d - Shaker table accelerometer
Note: Seismic mass, M, supported by mandrels contains accelerometer within

Fig. 3. Block diagram of the experimental apparatus. The rubber springs for vibration isolation are connected to an isolated concrete table, which straddles the shaker table and test fixture towers.

principle zero if the two mandrels are identical. A displacement which is orthogonal to the sensor axis causes both mandrels to be extended by the same amount hence generating no optical path length difference. If the sensitivity of the individual mandrels are not identical, transverse displacement will generate a signal which is proportional to the sensitivity difference of the two mandrels multiplied by a small quantity which is second order in the orthogonal displacement.

While the length of the individual interferometer arms must be identical to within the coherence length of the light source in order to produce good fringe visibility, there are no similar constraints on the transmission fibers which are on the opposite side of the coupler that provide light and return the modulated interferometer signal, so the sensor can exploit existing fiber-optic communications technologies to bring light to the sensor and return the signal to the photodetector without noise in these fibers contributing to the seismically induced phase shifts. Electrooptical conversion can occur at the observer location, even for very large sensor–receiver separation distances.

B. Mandrel Characteristics

The rubber mandrels used in the experiments reported here were cast from two materials, one (Eccosil® 2CN) having an effective Young's modulus of 3.9×10^6 dyn/cm^2 and the other (Eccosil® 5019) an effective Young's modulus of 1.2×10^7 dyn/cm^2. Both materials were mixed and degassed before being poured into molds and cured at 60°C to reduce curing time.

Fig. 4 is a diagram of the mandrel geometry used to calculate mandrel stiffness and sensor optical phase shift. Due to the design of the chucks used for winding the mandrels, a small region at either end could not be wrapped. The net result is that the model is characterized by three springs in series, two being the unwrapped portion of the

®Registered service mark of the Emerson & Cuming Co., Canton, MA.

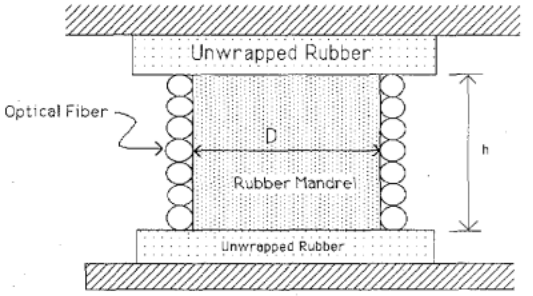

Fig. 4. Model geometry used to calculate mandrel stiffness and optical sensitivity.

mandrel and the other the stiffness afforded by the central portion of the mandrel constrained by the optical fiber. The calculations of mandrel stiffness and optical sensitivity presented in this section treat only fully wrapped mandrels. The contributions of the unwrapped portions, and the differences between theoretical and measured values of the effective spring constant for the mandrels, will be treated in a later section.

The effective spring constant of a fully wrapped mandrel is calculated by assuming that the elastic energy stored by the deformation of the mandrels can be cast in two different, but equivalent, forms. The first form is an expression for the stored elastic energy in the optical fiber, and the second is for energy stored in the mandrel proper when treated as a spring.

The stiffness of the fiber is length dependent, in that, given equal extension, a long piece of fiber experiences less strain than does a short piece of fiber. Therefore, the stiffness of the fiber is inversely proportional to its length and can be written as

$$K_f = \frac{K_{fn}}{N\pi D} \tag{4}$$

where

- K_{fn} stiffness of one unit length, of optical fiber (the stiffness-length product),
- K_f effective fiber stiffness,
- $N\pi D$ total fiber length, and
- N number of circumferential wraps of fiber.

The total fiber energy E_f is

$$E_f = \frac{1}{2}\frac{K_{fn}}{N\pi D}(\delta L)^2 \tag{5}$$

where $\delta L = N\pi\delta D$, the fiber extension.

The equation for the total potential energy stored in the fiber wrapped portion of the mandrel is

$$E_f = \frac{K_{fn}}{2N\pi D}(N\pi\delta D)^2$$

or

$$E_f = \frac{N\pi K_{fn}}{2D}(\delta D)^2. \tag{6}$$

The potential energy stored in the mandrel can similarly be written as a function of mandrel stiffness, in that a change in mandrel height results in the same energy being stored. Recalling the assumption of volume conservation

$$V = \frac{\pi D^2 h}{4}$$

therefore

$$-\frac{2\delta D}{D} = \frac{\delta h}{h}$$

or

$$\delta h = -\frac{2h\delta D}{D} \tag{7}$$

where h is the height of the fiber wrapped portion of the mandrel and

$$E_m = \tfrac{1}{2}K_m(\delta h)^2$$

or using (7)

$$E_m = \frac{2h^2K_m}{D^2}(\delta D)^2 \tag{8}$$

where K_m = effective mandrel stiffness constant for a single mandrel.

Equating the two expressions for the potential energy $E_m = E_f$ the effective mandrel stiffness constant can be cast as a function of the stiffness of one unit length of the fiber and the mandrel dimensions or

$$K_m = \frac{N\pi D}{4h^2}(K_{fn}). \tag{9}$$

This result can be exploited to generate an expression for the resonance frequency of the seismic sensor which consists of a mass supported by two mandrels as shown in Fig. 2:

$$f_n = \frac{1}{2\pi}\sqrt{\frac{2K_m}{M}}$$

or

$$f_n = \sqrt{\frac{NDK_{fn}}{8\pi h^2 M}}. \tag{10}$$

C. Optical Sensitivity Calculation and Optical Leverage

The optical phase shift measured by the interferometer is a function of the optical path length difference. The phase shift in one mandrel resulting from this deformation is given by

$$\delta\Psi = \frac{2\pi\eta}{\lambda_0}\delta L \tag{11}$$

where

- $\delta\Psi$ optical phase shift,
- λ_0 light wavelength in vacuum,
- η index of refraction of the fiber core,
- δL total change in fiber length.

Using (7) developed in the previous section, and (11), the theoretical optical phase shift as a function of mandrel height change can be written as

$$\frac{\delta\psi}{\delta h} = \frac{\eta\pi^2 ND}{\lambda_0 h}. \tag{12}$$

The total phase shift in the seismometer is given when (12) is multiplyed by a factor of four, two because of the Michelson configuration, and two because the mandrels operate in a push–pull fashion.

By combining (11) and (12) we can express the optical sensitivity as an effective optical leverage, that is, the ratio of the overall change in optical path length to the change in the position of the seismic mass

$$\frac{\delta L}{\delta h} = \frac{2\pi ND}{h}. \tag{13}$$

For the sensors described herein this optical leverage is of order 10^3.

Using the optical leverage, the sensitivity of the sensor when operating in the accelerometer limit can be modeled by using Hooke's Law, where the force/distance proportionality factor is $2K_m$, and Newton's Second Law, where the force/acceleration proportionality factor is the seismic mass, to form the ratio between the total optical phase shift and the acceleration:

$$\frac{\delta\psi}{\delta\alpha} = \frac{8\pi\eta hM}{\lambda_0 K_{fn}}. \tag{14}$$

IV. Measurements

A. Stiffness

As demonstrated earlier, the ratio of the operating frequency to the resonant frequency determines the behavior of the seismic instrument. In the seismometer limit the sensor must operate above resonance, which is a function of both the mandrel stiffness and the seismic mass. For the case of interest, the mandrel stiffness is directly proportional to the optical fiber stiffness, (9), since the rubber acts only as a transformer. To test the model, both rubber elasticity and fiber stiffness were measured.

The effective fiber stiffness was measured using a slide weight which was dropped a short distance onto a platform containing a piezoelectric accelerometer which was, in turn, suspended from an optical fiber. The free-decay response was recorded on a digital storage oscilloscope. Four slide masses were used to excite the longitudinal mode in the fiber thereby allowing the determination of the measured stiffness by a least squares fit. The free decay frequencies decreased with increasing mass thereby insuring that the vibrational mode was longitudinal rather than transverse (as in a guitar). The stiffness-length product for the Corning 80-μm single mode fiber used in this study was found to be $(3.36 \pm 0.04) \times 10^7$ dyn which agrees well the 3.8×10^7 dyn calculated using nominal

TABLE I
TABULATION OF THE MANDREL STIFFNESS FOR FOUR SENSORS. Sensor number is in parentheses. The measured stiffness increases with increasing number of wraps of optical fiber.

Mat'l (Sensor)	Diam (cm)	Height (cm)	No. Wraps	Wrap Height	K_m (dynes/cm $\times 10^7$)	K_{meas}
2CN						
	3.74	2.20	0	N/A		3.7
(4)	3.74	2.20	78	1.78	246	74.2
(6)	3.98	2.18	85	1.92	245	106
5019						
	3.78	2.30	0	N/A		9.7
(5)	3.78	2.30	77	1.84	230	76.8
(7[a])	3.7	2.2	82	1.98	208	114

[a]The fiber on this mandrel was encapsulated within the rubber. All other mandrels had the fiber wrapped externally.

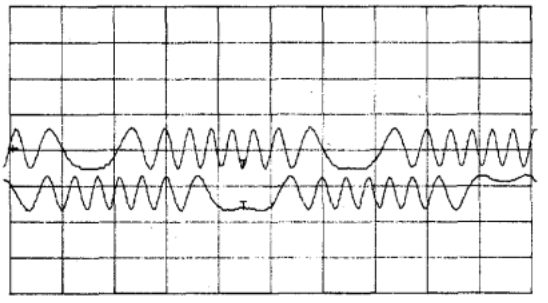

Fig. 5. Photodetector output as measured on the digital oscilloscope. The upper trace is for an ac coupled signal, and the lower for a dc coupled signal. The center line is approximately ground potential.

values for the Young's modulus for glass [6]. The 80-μm optical fiber used in this study was selected in lieu of the more common 125-μm fiber because of its lower bending loss and lower stiffness.

The characteristics of the fiber wrapped and unwrapped mandrels were measured statically using an Instron Model 1102 compression testing machine and dynamically by both free-decay frequency measurements similar to those used to characterize the fiber above and resonance frequency measurements using the apparatus in Fig. 3. Those results are summarized in Table I. In summary, the wrapped mandrels were more stiff than the bare mandrels by factors of approximately 10 to 30 depending on the type of rubber and the number of wraps of fiber. Clearly, the stiffness of the mandrels is controlled by the stiffness of the optical fiber. Note that as the wrapped fraction of the mandrel increases (Table I), the measured stiffness approaches the calculated value K_m.

B. Optical Sensitivity Measurements

Initially, the optical phase shift measurements were made by increasing the vibration amplitude of the shaker table until the magnitude of the optical signal at the shaker table frequency was zero. This null occurs when the optical phase shift equals 3.8317 rad corresponding to the first zero in the first order Bessel function [7]. However, as the sensors incresed in sensitivity, this technique became intractable since the shaker table vibration amplitude required was so small.

The technique by which the bulk of the measurements reported here were made was by fringe-counting. The shaker table drive signal is provided by the impedance analyzer (Fig. 3). Table displacement is measured using the table accelerometer, Ithaco preamplifier, and dual channel spectrum analyzer. The photodetector signal was recorded on the digital oscilloscope and the number of peaks or valleys (fringes) counted. A sample of the output is shown in Fig. 5. The upper trace in Fig. 5 is an ac coupled signal, and the lower trace a dc coupled signal. The center grid line is approximately ground potential. Adjacent peaks represent 2π rad of optical phase shift. Fractions of a fringe can be estimated accordingly. The regions of no change in optical phase shift represent the table displacement maxima. Regions with rapid change in phase represent the greatest rate of change of the fiber length, or a table velocity maximum.

A sensitivity measurement at each frequency was made with several values of drive amplitude applied to the shaker table; the variation in sensitivity at individual frequencies due to differing excitation levels was typically less than 3 percent due primarily to the errors associated with estimates of fractional fringes. This small deviation demonstrates that the sensor response is nearly linear, even with foundation displacements four orders of magnitude greater than those expected in service.

V. RESULTS AND DISCUSSION

A. Seismometer and Accelerometer Sensitivity

Several sensors were constructed and evaluated. Table I summarizes the mandrel stiffness values and their physical dimensions. In general, the later sensors were wrapped with more fiber as materials become available and the wrapping technique was refined. Accordingly, these sensors are more sensitive due to the greater optomechanical interaction region, although the stiffness and attendent resonance frequency also increases.

The measured optical sensitivity data for the sensor is presented as Fig. 6, and is compared to the theoretical limit for the geometry and wrapping density of Sensor 5 in Table I. While the theoretical limit assumes a stationary seismic mass, the mass in the actual sensor exhibited displacements approximately 30 percent of the shaker table displacement at frequencies well above resonance. The theoretical value is calculated via (12) and multiplied by a factor of four due to the Michelson configuration and the push–pull nature of mandrel deformation.

The sensor when operated below resonance performs as an accelerometer (3). Fig. 7 is a plot of the sensor sensitivity versus frequency when operated as an accelerometer, with a 542-gm seismic mass and a 100-gm seismic mass and again agreement with theory is good.

B. Optical Comparator Measurements

The discrepancy between the model predictions and measured values for stiffness and optical sensitivity can

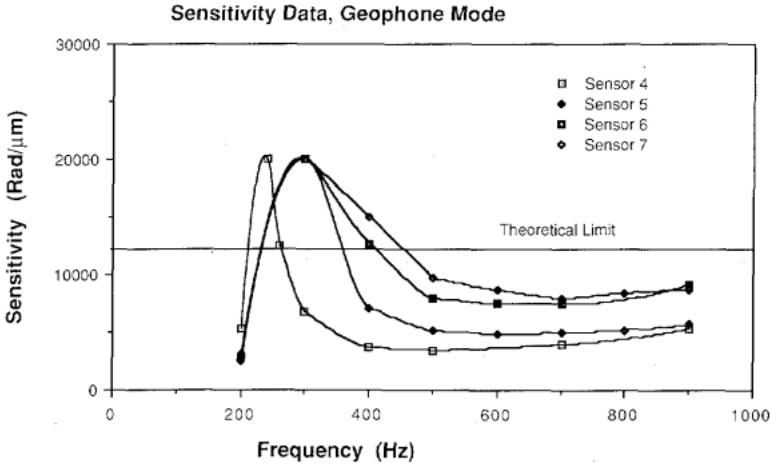

Fig. 6. Optical sensitivity for four sensors compared to the theoretical seismometer limit for Sensor 5. The theoretical sensitivity is 11 100 rad/μm. The lines through the data points are to guide the eye. The response below resonance is shown in Fig. 7.

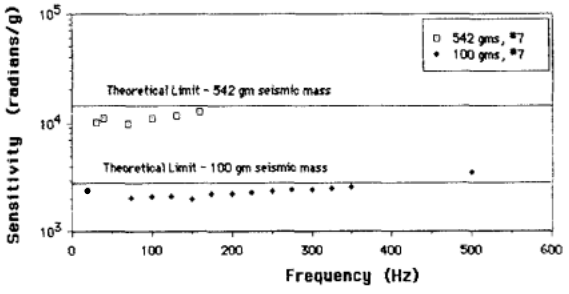

Fig. 7. Accelerometer sensitivity versus frequency for Sensor 7 compared to the theoretical accelerometer limit with seismic masses of 100 gm and 542 gm.

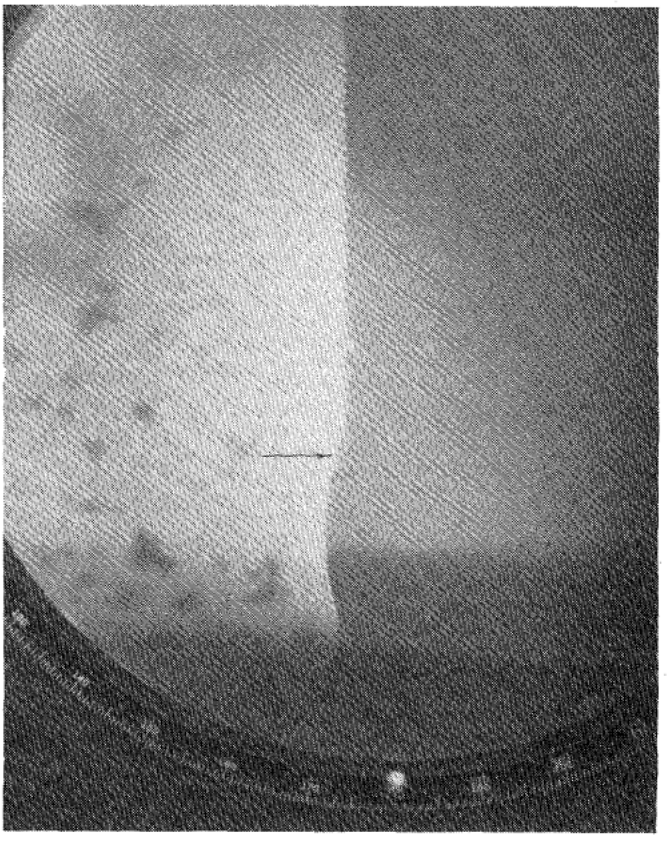

Fig. 8. Mandrel diametrical change versus height change as viewed on an optical comparator. The transition region between the fiber wrapped section and unwrapped section is idicated by the arrow.

be explained by recognizing that the mandrel does not have three distinct and separable regions (Fig. 4) contributing to the stiffness. The assumption that the rubber is incompressible is thought to be reasonable, but there is a transition where the fiber at the limits of the wrapped region is strained more than the fiber on the remaining portion of the mandrel, as evident in the photograph of a strained mandrel in an optical comparator shown in Fig. 8. Additionally, for the mandrel shown, the unwrapped portion of the mandrel is approximately 15 percent of the mandrel height, and approximately 30 percent of the height change occurs in this region. Accordingly, the diameter change in the wrapped region is smaller than the theory assumes, as the height change of the mandrels is distributed throughout the mandrel rather than being confined to the region constrained by the fiber. In treating the unwrapped portions as independent springs using elastic theory for rubberlike materials [9], the calculated equivalent stiffness was at least a factor of 5 greater than observed. That theory is believed to fail with diameter-to-height aspect ratios present in the mandrels tested, as the modulus equations does not converge to the modulus of unilateral compression for extremely high aspect ratios.

Using values for diametrical change with height change observed with an optical comparator, the measured stiffness (Sensor 5) is lower than the stiffness calculated from the fiber deformation by approximately 15 percent. The optical sensitivity calculated from the measured diametrical change agrees with the total theoretical value to within 20 percent, and is high. These results are consistent in that a higher value of stiffness calculated from comparator data implies greater diametrical expansion, which requires more fiber stretch. The additional fiber stretch

implies greater optical path length difference which is reflected in a higher sensitivity. Mandrel designs permitting full wrapping are presently under investigation.

C. Intrinsic (Thermal) Noise and Minimum Detectable Signal

The transduction process in a fiber-optic interferometric sensor occurs in two stages: opto-mechanical conversion followed by electrooptic conversion. That is, first the mechanical deformation of the fiber is converted into an optical phase shift (e.g., radians per gram or radians per micrometer), then the optical phase shift is converted into an analogous electrical signal by an interferometric demodulator, which consists of photodiodes, amplifiers, signal processing electronics, etc., to produce a given voltage per radian of optical phase shift. Although both of these processes introduce noise into the measurement, only the electrooptic demodulation noise has been treated in the literature [1], [2], [5], [9]–[11]. This deficiency has not caused any difficulty to date because the optical sensitivity of the sensors has not been large and most sensor systems have been plagued by other noise problems and measurements in low noise environments have not been attempted. With a sensor such as the one described herein, the intrinsic thermal noise of the mechanical portion of the sensor is of the same order as the published values for demodulator noise figures (e.g., ≈ 1–$100\ \mu\text{rad}/\sqrt{\text{Hz}}$) in the frequency range of interest (10–1000 Hz).

A calculation of the intrinsic (thermal) noise in fiber-optic mechanical sensors is beyond the scope of this article and will be presented in detail elsewhere [12]. The problem is isomorphic to that of thermal noise in a conventional galvanometer which employs a mirror to produce an optically leveraged output signal [13]. The calculation of the root-mean-square thermal displacement is obtained trivially via the equipartition theorem [14] by equating the thermal energy to the elastic energy (8). The measured opto-mechanical sensitivity of the sensor converts this displacement noise to a phase noise. The equivalent phase noise spectral density can then be obtained because the rms thermal displacement is the integral over frequency of the product of an assumed "white" spectral density for the thermal forcing function and the squared modulus of the transfer function which is of the form of (2) [15]. For the sensors described here the phase noise spectral density below resonance is approximately 10 $\mu\text{rad}/\sqrt{\text{Hz}}$ and falls off above resonance at 12 dB/octave. The rms phase noise is approximately 450 μrad, most of which occurs within the -3-dB bandwidth about resonance.

D. Comparison to Other Fiber-Optic Accelerometers

Assuming the intrinsic (thermal) noise dominates, the sensor's minimum detectable signal in the accelerometer limit is approximately 1 $\text{ng}/\sqrt{\text{Hz}}$. This is approximately 20 dB better than the minimum detectable signal obtainable with the best available conventional vibration sensor [16] and 20 dB more sensitive the best previously reported high-sensitivity fiber-optic accelerometer [17].

References

[1] T. G. Giallorenzi, J. A. Bucaro, A. Dandridge, G. H. Sigel, Jr., J. H. Cole, S. C. Rashleigh, and R. G. Priest, "Optical fiber sensor technology," *IEEE J. Quantum Electron.*, vol. QE-18, no. 4, pp. 626–665, 1982.

[2] V. I. Busurin, A. S. Semenov, and N. P. Udalov, "Optical and fiber-optical sensors (review)," *Sov. J. Quantum Electron.*, vol. 15, no. 5, pp. 595–621, 1985.

[3] K. Tanaka, "How to detect the gravitationally induced phase shift of electromagnetic waves by optical-fiber interferometry," *Phys. Rev. Lett.*, vol. 51, no. 5, pp. 378–380.

[4] C. M. Harris and C. E. Crede, Ed., *Shock & Vibration Handbook*. New York: McGraw-Hill, 1976.

[5] C. M. Crooker and S. L. Garrett, "Fringe counting demodulator for fiber optic interferometric sensors," *J. Acous. Soc. Amer.*, vol. 80, no. S1, p. S26, 1986.

[6] D. E. Gray, Ed., *American Institute of Physics Handbook*, 3rd Ed. McGraw-Hill, 1972.

[7] G. B. Mills, S. L. Garrett. and E. F. Carome, "Fiber-optic gradient hydrophone," *Proc. Soc. Photo-Optical Eng.*, vol. 478, pp. 98–103, 1984.

[8] J. C. Snowden, *Vibration and Shock In Damped Mechanical Systems*. New York: Wiley, 1968.

[9] K. P. Koo, A. B. Tveten and A. Dandridge, "Passive stabilization scheme for fiber interferometers using (3×3) fiber directional couplers," *Appl. Phys. Lett.*, vol. 41, p. 616, 1982.

[10] T. K. Stanton, R. G. Pridham, W. V. McCollough, and M. P. Sanguinetti, "On fiber-optic hydrophone noise-equivalent pressure," *J. Acous. Soc. Amer.*, vol. 66, no. 6, pp. 1893–1894, 1979.

[11] T. K. Stanton, "Noise-equivalent pressure of a single-fiber interferometric acoustic sensor," *J. Acous. Soc. Amer.*, vol. 69, no. 1, pp. 311–312, 1981.

[12] T. Hofler and S. L. Garrett, "Thermally induced intrinsic phase noise in a fiber optic interferometric seismic sensor," submitted for publication.

[13] C. W. McCombie, "Fluctuation theory in physical measurement," *Rep. Progress Phys.*, vol. 16, pp. 266–320, 1953.

[14] F. Reif, *Fundamentals of Statistical and Thermal Physics*. New York: McGraw-Hill, 1965, p. 249.

[15] C. Kittel, *Elementary Statistical Physics*. New York: Wiley, 1958, p. 30.

[16] Wilcoxon Research, Rockville, MD, Model 731 Seismic Accelerometer.

[17] A. D. Kersey, D. A. Jackson, M. Corke, "High-sensitivity fiber-optic accelerometer," *Electron. Lett.*, vol. 18, no. 13, p. 559, 1982.

*

David L. Gardner was born in Beverly, MA, on Sept. 20, 1944. He received the B.S. (1972) and M.S. (1976) degrees in ocean engineering from Florida Atlantic University, with a specialization in acoustics.

He has worked with the U.S. Army, General Dynamics, Electric Boat Division as a Nuclear Projects Engineer, and, for the past ten years with the NOAA Commissioned Corps specializing in oceanic instrumentation design and field experimentation. He is presently working towards the Ph.D. degree in engineering acoustics at the Naval Postgraduate School.

Mr. Gardner is a member of Acoustical Society of America.

*

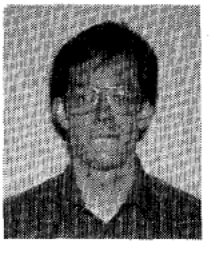

Thomas Hofler was born in Mason City, IA, on February 11, 1955. He received the Sc.B. degree in physics from Brown University in 1977. He received the Ph.D. degree in physics from the University of California, San Diego, in 1986, for graduate research conducted at Los Alamos National Laboratory on thermoacoustic heat engines.

Steven R. Baker was born in Los Angeles, CA, on March 19, 1953. He received the B.S. (1975), M.S. (1977), and Ph.D. (1986) degrees in physics from the University of California, Los Angeles, specializing in the acoustic properties of superfluid helium.

Since 1985, he has been at the Naval Postgraduate School, where he is an Assistant Professor in Physics. His research interests include the acoustics of fluid-filled porous media and transduction.

Dr. Baker is a member of the American Physical Society, the Acoustical Society of America, Sigma Xi, and the Audio Engineering Society.

*

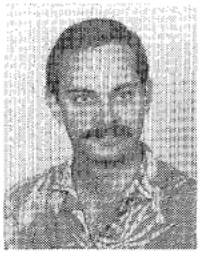

R. K. Yarber was born in Spokane, WA, on July 2, 1954. He completed the U.S. Navy Electronic Warfare Technician School in 1977 and has completed a tour in the Operations Department of the USS California (CGN-36).

He is currently a Chief Petty Officer in the Naval Reserves, and an Engineering Technician and part-time student at the Naval Postgraduate School working on the B.S. degree in physics. He is a student member of the Acoustical Society of America.

Steven L. Garrett was born in Los Angeles, CA, on April 3, 1949. He received the B.S. (1970), M. S. (1972), and Ph.D. (1977) degrees in physics from the University of California, Los Angeles with specializations in quantum fluids, condensed matter physics, and acoustics.

After completing his degree he received the F.V. Hunt Fellowship of the Acoustical Society of America and spent a year in England at the University of Sussex experimenting with thermohydrodynamics of superfluid ^{3}He. This was followed by two years of ultralow temperature research in the Physics Department of the University of California, Berkeley, as a Fellow of the Miller Institute for Basic Research in Science. Since 1982 he has been at the Naval Postgraduate School in Monterey, CA, where he is an Associate Professor of Physics. He spent his sabbatical as the Rosen Professor of Solid-State Physics at the Israel Institute of Technology in Haifa, Israel, in 1985, and has been a Visiting Scientist at the Los Alamos National Laboratories since 1981. His current research interests include thermoacoustic engines, reciprocity calibration of electroacoustic transducers, fiber-optic sensor systems, and various acoustical consulting projects.

Dr. Garrett is a member of the American Physical Society, the Acoustical Society of America, and the Optical Society of America.